Contents lists available at ScienceDirect

Materials Today Bio

journal homepage: www.journals.elsevier.com/materials-today-bio

Nerve guidance conduit design based on self-rolling tubes

T.B. Aigner [a,g], C. Haynl [a,g], S. Salehi [a], A. O'Connor [b], T. Scheibel [a,c,d,e,f,*]

[a] *University of Bayreuth, Department of Biomaterials, Prof.-Rüdiger-Bormann-Str.1, 95447, Bayreuth, Germany*
[b] *University of Melbourne, Department of Biomedical Engineering, Melbourne, Victoria, 3010, Australia*
[c] *University of Bayreuth, Bayreuther Zentrum für Kolloide und Grenzflächen (BZKG), Universitätsstraße 30, 95447, Bayreuth, Germany*
[d] *University of Bayreuth, Bayreuther Zentrum für Molekulare Biowissenschaften (BZMB), Universitätsstraße 30, 95447, Bayreuth, Germany*
[e] *University of Bayreuth, Bayreuther Materialzentrum (BayMAT), Universitätsstraße 30, 95447, Bayreuth, Germany*
[f] *University of Bayreuth, Bayerisches Polymerinstitut (BPI), Universitätsstraße 30, 95447, Bayreuth, Germany*

ARTICLE INFO

ABSTRACT

The current gold standard in peripheral nerve repair is nerve autografts for bridging gaps larger than a centimeter. However, autografts are associated with a low availability and the loss of function at the donor site. Nerve guidance conduits (NGCs) made of biocompatible and biodegradable materials reflect suitable alternatives. Clinically approved NGCs comprise either wraps that are rolled around the loose ends of the nerve or steady-state tubes; however, both lack internal guidance structures. Here, we established self-rolling NGCs to allow for gentle encapsulation of nerve cells together with supportive microenvironments, such as (1) an inner tube wall coating with a bioactive spider silk film, (2) an inner tube wall lining using an anisotropic spider silk non-woven mat, or (3) a luminal filler using an anisotropic collagen cryogel. Neuronal cells adhered and differentiated inside the modified tubes and formed neurites, which were oriented along the guidance structures provided by the spider silk non-woven mat or by the fibrillary structure of the collagen cryogel. Thus, our size-adaptable NGCs provide several features useful for peripheral nerve repair, and distinct combinations of the used elements might support and enhance the clinical outcome.

1. Introduction

Peripheral nerve injuries, such as crushes or sections, can be consequences of vehicle or industrial accidents, falls, or penetrating trauma [1]. The peripheral nervous system in vertebrates reacts to such injuries by active degeneration and regeneration [2,3]. Problematic are gaps, which are larger than 1 cm, thus, original nerve function cannot be restored using bioinert nerve guidance conduits (NGCs) [4,5]. In those cases, the current gold standard is nerve autografts, providing the extracellular matrix, viable Schwann cells, and growth factors needed for optimal regeneration [6–8]. Therewith, a physical guidance is given, allowing the nerve tissue cells to sprout their axons from the proximal end to the distal stump [9]. Unfortunately, the number of supplies in donor nerve tissue is limited and nerve removal causes a loss of function at the donor site. Further, a complete functional restoration cannot be guaranteed at the acceptor site [6,10]. An alternative to nerve autografts is using artificial NGCs [11–13].

Basically, there are several properties the NGC has to meet to increase the success of the clinical outcome. The NGC must be biocompatible and biodegradable to not provoke any immunological reaction or other side-effects and to avoid compression caused by non-degraded components [13]. The NGC must be flexible and soft because the gap to be bridged might cross a joint but at the same time should possess enough stability to be implanted by surgeons [13]. NGCs, which are mostly based on tubular structures, should be semipermeable allowing the diffusion of gases and nutrients but should avoid infiltration of inflammatory cells and scar tissue formation. Furthermore, the presence of bioactive molecules and adhesion of supporting cells, such as, for instance, Schwann cells, has been found to be crucial [11–14].

Filler materials within the tubular structure can create a cell friendly microenvironment promoting cell adhesion, proliferation, migration and differentiation, and directed growth of neuronal cells and their neurites. For instance, multilumen or microporous fillers, hydrogels or fiber containing conduits, and microgrooves or nanoimprints on the inner wall have been under investigation [11,12]. Another possibility is the use of

cryogels, which provide a three-dimensional environment [15,16] favorable for this application.

Clinically approved NGCs are either wraps that are rolled around the loose ends of the nerve or steady-state tubes, in which both nerve ends are inserted [17]. Those NGC variants are not modified with internal guidance structures and they are made of either synthetic polymers, such as polyglycolic acid (Neurotube®), polylactide-caprolactone (Neurolac™) and polyvinyl alcohol (Salutunnel™), or collagen type I (NeuraGen®, NeuraWrap™, NeuroMend™, NeuroMatrix™, Neuro-Flex™) [17], which is an extracellular matrix protein also found in peripheral nerves, providing myelinated axons with functional support [12,18,19] and generally exhibiting excellent biocompatibility, extremely low immunogenicity, chemotaxis, and biodegradability [20, 21].

Besides collagen, other naturally derived materials such as chitosan and spider silk are promising candidates for NGC fabrication because of their excellent compatibility with the human body. Chitosan is a derivative of naturally occurring chitin, a by-product of the seafood industry. It shows antimicrobial properties [22] and is used in food, cosmetics, and pharmaceutical and biomedical applications [23, 24], including peripheral nerve repair [25,26]. Natural spider silk fibers exhibit remarkable mechanical properties [27,28] and have performed well in *in vivo* peripheral nerve repair studies [29,30]. Owing to the difficulties (i.e., cannibalism) in spider farming, which prevent the production of large amounts and a constant material quality [31], recombinant spider silk proteins can nowadays be provided, and materials made thereof have exhibited suitable properties in neuronal *in vitro* tests [32–34]. Recombinant spider silks can be processed into several tailorable morphologies, for example, films, foams, non-woven mats, or hydrogels [35–42], and these materials were shown to not induce an immune response in the body and to degrade rather slowly [43–46]. In comparison with electro-spun collagen nanofibers, recombinant spider silk nanofibers are less prone to swelling [47], allowing a higher degree of nerve cell orientation along the fiber axes. Furthermore, different modifications are possible on the genetic level, for instance, the introduction of an arginine—-glycine-aspartic acid (RGD)-bearing cell binding motif [48].

We have recently shown the application of self-rolling tubes as containers for enzymatic reactions [49]. In the present study, we designed a biocompatible and biodegradable self-rolling tubular NGC. Although the commercially available NeuroMend™ exhibits self-rolling properties, its lack of internal structures, which would be beneficial for cell vitality and differentiation, as well as directed nerve growth and neurite elongation, is regarded as one severe drawback limiting the success of the clinical outcome. Therefore, we studied the benefit of a self-rolling tube made of chitosan and different filler morphologies, which adapts to the dimensions of the injured peripheral nerve upon rolling around the loose ends and the filler material. It could be shown that the new NGCs ensured the viability of neuronal cells during encapsulation. In this study, all variants tested allowed differentiation of neuronal PC-12 cells within the NGCs, and anisotropic structures provided guidance of neurites. Our study combines the usefulness of the self-rolling property of a tube with the incorporation of suitable internal morphologies and is therefore of high importance to the development of new materials for peripheral nerve repair.

2. Materials and methods

2.1. Fabrication of self-rolling chitosan films

A filtered chitosan solution (1% w/v in 2% v/v formic acid, 190–310,000 g mol^{-1}, Sigma-Aldrich) was cast into a Petri dish (Sterilin™, diameter: 90 mm) yielding a density of 2.36 mg cm^{-2}, and the film was air dried overnight. This film was post-treated with 0.2 M NaOH for 5 min and subsequently washed with ultrapure water.

2.2. Fabrication of self-rolling chitosan films with an internal eADF4(C16)-RGD coating

The preparation of self-rolling chitosan tubes with an internal spider silk eADF4(C16)-RGD coating was conducted according to Aigner and Scheibel [49]. In brief, an eADF4(C16)-RGD [48] solution in 1,1,1,3,3, 3-hexafluoro-2-propanol (HFIP, 8.33 mg ml^{-1}, 0.08 mg cm^{-2}, 48, 583 g mol^{-1}) was cast into a Petri dish (Sterilin™, diameter: 90 mm) and, after drying, post-treated with 70% (v/v) ethanol to render the silk film to be insoluble in water by inducing β-sheet formation. Then, a chitosan film was cast on top of the eADF4(C16)-RGD film according to the procedure outlined in Section 2.1.

2.3. Fabrication of self-rolling chitosan films with an internal eADF4(C16) anisotropic non-woven mat

A chitosan film was prepared as depicted in 2.1 and removed from the Petri dish and fixed on a rotating drum with double-sided tape. The rotating drum allowed production of aligned fibers yielding an anisotropic non-woven mat. Electrospinning of eADF4(C16) was performed according to the study by Lang [50]. A 150 mg ml^{-1} solution of eADF4(C16) (47, 698 g mol^{-1}, AMSilk GmbH) in HFIP was electrospun onto the chitosan film (voltage: 30 kV; distance to collector: 15 cm; flow rate: 300 μl min^{-1}; relative humidity: 50%). The spider silk non-woven mat was post-treated first in pure ethanol vapor for 3 h, followed by a treatment in 90% ethanol in the vapor phase (corresponds to 87% v/v ethanol) for 2 h to render the mat to be insoluble in water and to obtain a tight connection between the spider silk non-woven mat and the chitosan film.

2.4. Fabrication of anisotropic collagen cryogels

Collagen type I extracted from calf skin (Sigma-Aldrich) was dissolved in 0.5% (v/v) acetic acid at pH 3 for 20 h. After centrifugation at 17,700 g for 10 min, the supernatant was removed and showed a collagen concentration of 4.8 mg ml^{-1}. Then, an aqueous glutaraldehyde solution (25% v/v in water, Carl Roth GmbH + Co. KG) was mixed with the collagen solution yielding a final concentration of 1% glutaraldehyde (v/v). This solution was then immediately transferred into a vertically standing plastic tube, which was tightly fixed to a copper plate. After sealing the top opening of the filled plastic tube with parafilm and mounting a thermal insulation (tube filled with cotton wool) on top, the whole setup was transferred into a −20 °C temperature freezer for 48 h. Subsequently, the frozen collagen cryogel precursor was pushed out of the tube into phosphate buffered saline (PBS), pH 7.4 at room temperature to neutralize the acidic pH, thereby preventing reversible dissolution of the collagen cryogel. After 20 h gelation in PBS, the collagen cryogel was washed three times with PBS containing 0.1 M glycine. The washing was continued using two further washing steps during the next 24 h to ensure complete capture of any free glutaraldehyde groups. Finally, the collagen cryogel was washed using PBS and stored in PBS until further experiments were carried out.

2.5. Chitosan tube formation

The underlying self-rolling mechanism of the used chitosan film was based on the difference of the swelling behavior between its bottom and top layer (Section 2.1). A more detailed explanation of this process can be found in the study by Ionov [51]. Here, chitosan films were cut into rectangles with desired sizes. The self-rolling process was induced by immersing this film into an aqueous solution, that is, into phosphate buffered saline (pH 7.4). However, self-rolling was induced as well in contact with cell culture medium, which resulted in entrapping the cell suspension. To encapsulate cryogels, they were placed on the film, which self-rolled forming a tube filled with cryogel. The tube diameter could be tailored to a certain extend by varying the film thickness and the diameter of the filler, for example, the cryogel.

2.6. Morphological characterization of NGCs

NGC components were analyzed using stereo microscopy (Leica M205C) and scanning electron microscopy (SEM; Sigma VP 300, Zeiss). For SEM, the samples were mounted on aluminum studs with adhesive carbon tape and then sputter coated with platinum (2 nm). Collagen cryogels were prepared for imaging by washing and storing them for further use in 10 mM ammonium hydrogen carbonate buffer. After flash freezing in liquid nitrogen, the collagen cryogels were placed in a lyophilization device (Alpha 1–2 LDplus, Christ) for one week. The cryogel cross-section was prepared in advance to flash freezing and lyophilization by cutting the soaked cryogel using a sharp razor blade.

2.7. Determination of water content and swelling degree of collagen cryogels

Collagen cryogels were prepared having 2 cm in length (number of samples n = 6). The weight of the fully soaked cryogels in PBS (m_{soaked}) and of the cryogels after removing unbound PBS with a paper tissue ($m_{removed}$) was determined using a microbalance (Practum 224-1S, Sartorius Lab Instruments). The water content in soaked cryogels was calculated using Eq. (1).

$$\text{water content of collagen cryogels } [\%] = (m_{soaked} - m_{removed}) / m_{soaked} \times 100 \tag{1}$$

The swelling ratio of the collagen cryogels was calculated using Eq. (2). Therefore, the diameter of the fully soaked cryogels was measured in PBS (V_{soaked}) and that of the cryogels after removing unbound water with a paper tissue ($V_{removed}$) using a stereo microscope (Leica M205C) (number of samples n = 4). The cryogels were assumed to be tubular, and their volumes were calculated using their diameter values.

$$\text{swelling ratio } [\%] = (V_{soaked} - V_{removed}) / V_{removed} \times 100 \tag{2}$$

2.8. Mechanical characterization of chitosan films and collagen cryogels

The chitosan films used for conduit fabrication and the collagen cryogels were analyzed using a tensile testing device (Bose Electroforce 3220) equipped with a 2.45 N load cell. Dry chitosan films were glued onto plastic frames using a high viscosity glue (UHU® Supergel), and they were immediately transferred into a fume hood for drying. The films on the frames were incubated in PBS before analysis using a strain rate of 0.05 mm s^{-1} (number of samples n = 5). Engineered stress of the films was calculated as the force divided by their cross-sectional areas assumed to be rectangular (film width × film thickness).

The mechanical properties of the collagen cryogel were analyzed referring to its longitudinal axis. Free PBS in collagen cryogels was removed using a paper tissue, and the diameters after this procedure were measured at three different positions. The moist cryogel was clamped between two plastic frames, applied to the tensile testing device, and measured at a strain rate of 0.05 mm s^{-1} (number of samples n = 4). Engineering stress of the cryogels was calculated as the force divided by the respective cross-sectional area, which was assumed to be circular. In terms of the films and the cryogels, the gauge length was adjusted to 2 mm. Strain was defined as the change in sample length divided by its original length. The Young's modulus was determined as the slope of the stress-strain plot in the linear elastic deformation range.

2.9. Seeding of PC-12 cells on the individual components and in the NGC

The different NGC components were prepared in untreated cell culture plates (24 wells, Thermo Fisher). For collagen surface treatment, the collagen type I solution (diluted 1:5 with sterile PBS, Cellmatrix®, Nitta Gelatin Inc) was used to coat the wells for 30 s. Then the solution was removed and the film was air dried. The eADF4(C16)-RGD film was cast directly into the wells using HFIP (33.3 mg ml^{-1}, 0.25 mg cm^{-2}) as a solvent. After drying, films were post-treated with 70% ethanol (v/v). The eADF4(C16) non-woven mats were prepared by electrospinning of a 150 mg ml^{-1} eADF4(C16) solution in HFIP onto plastic coverslips (12 mm diameter, Thermo Fisher). The same spinning and post-treatment conditions were used as explained in section 2.3. A fixation of the plastic coverslips onto the rotating drum for fiber alignment was not possible, thus, an isotropic non-woven mat was spun onto the coverslips. The collagen cryogel was glued into well plates using a silicon glue.

The neuronal cell line PC-12 (ATCC® CRL1721™) [52] was cultured in the growth medium (Dulbecco's Modified Eagle's Medium (DMEM) with 10% (v/v) heat inactivated horse serum (Gibco), 5% (v/v) fetal bovine serum (FBS, Merck), 1% (v/v) GlutaMAX (Gibco), 1% (v/v) penicillin/streptomycin (10,000 U ml^{-1}, Thermo Fisher), 20 mM 4-(2-hydroxyethyl)-1-piperazineethanesulfonic acid buffer (HEPES, Carl Roth)). For the adhesion test, 25–30,000 cells were seeded per square centimeter on the aforementioned materials and allowed to adhere for 7 days with medium changes on day 3 and 5. Treated cell culture plates were used as control. After 1, 3, and 7 days, cell morphology was observed using bright field microscopy (Leica DMi8).

2.10. Differentiation of PC-12 cells on NGC components

A density of 10,000 cells cm^{-2} were cultured on the aforementioned materials and incubated in the growth medium. After 1 day of culture, the growth medium was exchanged with the differentiation medium (DMEM with 2% (v/v) horse serum, 1% (v/v) GlutaMAX, 1% (v/v) penicillin/streptomycin, 20 mM HEPES buffer, 100 ng ml^{-1} nerve growth factor (NGF, 2.5s Native Mouse Protein, Thermo Fisher)), which was changed on day 3 and 5 of differentiation. After 7 days of differentiation, the cells were immunostained for detecting endogenous levels of β-III tubulin, and neurite outgrowth was evaluated. The staining procedure was as follows: cells were fixed with formaldehyde (Carl Roth; 3.7% in water, 15 min, at room temperature) and made permeable with Triton x-100 (Carl Roth; 0.3% (v/v), 5 min, at room temperature). A glycine solution (Carl Roth, 300 mM, 10 min, at room temperature) was added to deactivate aldehydes. Bovine serum albumin (BSA) blocking buffer was applied (Carl Roth; 5% (w/v), 30 min, 37 C) before adding the image enhancer (30 min, 37 C) of the Alexa Fluor™ 488 Goat Anti-Rabbit SFX Kit (Thermo Fisher). Then, the samples were incubated in primary polyclonal antibody anti-β-III tubulin (Abcam, rabbit; 1000 x diluted in 0.1% (w/v) BSA buffer, overnight, 4 °C). On the next day, cells were stained using the secondary antibody goat-anti-rabbit with an Alexa Fluor 488 label (Sigma-Aldrich; 1000 x diluted in 0.1% (w/v) BSA buffer, 1 h, 37 °C) and Hoechst (Invitrogen; 1000 × diluted in 0.1% (w/v) BSA buffer, 1 h, 37 °C). Imaging was performed using a fluorescence microscope (Leica DMi8). For cryogels, Z stacks were taken and overlaid using the maximal projection option provided by the software (LAS X 3.6.0).

2.11. Encapsulation of cells in tubes

Tube materials were cut to rectangular shapes (1.5 × 0.5 cm for pure chitosan, eADF4(C16)-RGD-chitosan and eADF4(C16) aligned fiber mat-chitosan tubes and 1.5 × 1 cm for chitosan tubes filled with the collagen cryogel), and the film thickness was determined to be 29.7 ± 3.0 μm [49]. These samples were allowed to roll in PC-12 cell suspension (10,000 cells ml^{-1}) to entrap the cells. In the case of the cryogel, the gel was first soaked in cell suspension and then applied on a chitosan film, which smoothly rolled around it. Collagen-coated cell culture plates were used as a positive control. After one day of culture, the medium was changed to differentiation medium. The differentiation medium was refreshed every two days. On day 7, cells were immunostained as described previously and analyzed using a wide field fluorescence microscope (Leica DMi8), and the images were processed using the software LAS X 3.6.0 by adjusting the brightness and the contrast. Z-stacks in combination with

the maximal projection mode were used to analyze all 3D samples. Importantly, cryogels were cut to slices giving a thickness of 1–3 cell layers (corresponding to 10–36 μm) and put on a glass slide covered with a coverslip to observe, whether adhered and differentiated cells could be found throughout all layers. Neurite length was determined by measuring neurites of nerve cells grown on each type of surface using ImageJ. The neurites were traced starting from their extrusion point from the cell body to the neurite's outer end, and this line was subsequently measured with the 'Measure' tool in ImageJ (collagen coating: 425 neurites, eADF4(C16)-RGD-coated tubes: 135 neurites, eADF4(C16) anisotropic non-woven mat tubes: 231 neurites, collagen cryogel in tube: 248 neurites). Then, the percentage of neurites was determined in each 10 μm length segment (0–10, 11–20, 21–30, and so on). Further, the number of cells in the images was counted using ImageJ 'Multi-point' modus to determine the neurite length per cell.

3. Results and discussion

### 3.1. Fabrication and characterization of NGCs

All NGC variants exhibited a tubular structure because of the used self-rolling chitosan film. The self-rolling mechanism has been recently described in Aigner and Scheibel [49] where the tubes were used as enzyme-reaction containers. The tubes could be prepared with various lengths (up to 10 cm), were stable between pH 3 and 11 and exhibited diffusion permeability with a molecular weight cutoff of 20,000 g mol^{-1}, which enables influx of nutrients, as well as gas exchange and metabolite removal. The self-rolling property of the chitosan film allowed an easy modification with other films or structured materials, the gentle and homogenous encapsulation of cells during rolling and, in principle, the

adaption of the tube size to the nerve ends or filler material.

To test the applicability of the self-rolling chitosan-based tubes for nerve regeneration, three variants of inner tube materials were tested to yield NGCs. An overview of the three NGC variants is schematically depicted in Fig. 1. Setup 1 used a hollow tube with an inner film coating made of the spider silk variant eADF4(C16)-RGD to provide a surface, where cells can efficiently adhere to; setup 2 used a hollow tube with an inner surface made of an anisotropic eADF4(C16) non-woven mat to provide a structure, where cells can adhere to and align on; setup 3 used a tube filled with a collagen cryogel with an anisotropic lamellar structure allowing cell adhesion and alignment. The first two NGCs (setups 1 and 2) possessed quasi-irreversible physical connection between the tube and the modifying materials. On the contrary, the collagen cryogel structure (setup 3) was not strongly connected to the chitosan tube, due to the processing conditions.

Upon fabrication of setups 1 and 2, rolling was induced by incubating the modified chitosan sheets with a PC-12 nerve cell suspension. For the preparation of setup 3, the cryogel was soaked in the PC-12 suspension and subsequently transferred onto the chitosan sheet, whereby immediate rolling of the sheet occurred and the encapsulation of the cryogel with cells was accomplished. The PC-12 cells were entrapped without applying mechanical stress, and they differentiated to form neurites, which has been previously shown to be crucial for peripheral nerve repair [53].

Fig. 2a,A shows the cross-section of a plain chitosan tube, and in Fig. 2a,B, the inner surface topography is presented. The chitosan tube soaked in PBS exhibited high transparency (Fig. 2a,C). Modifying the chitosan inner tube wall with an eADF4(C16)-RGD film yielded biofunctionalization, which was not visible in the cross-section because of its low thickness (Fig. 2b,A). In the particular case, the poor solubility of the
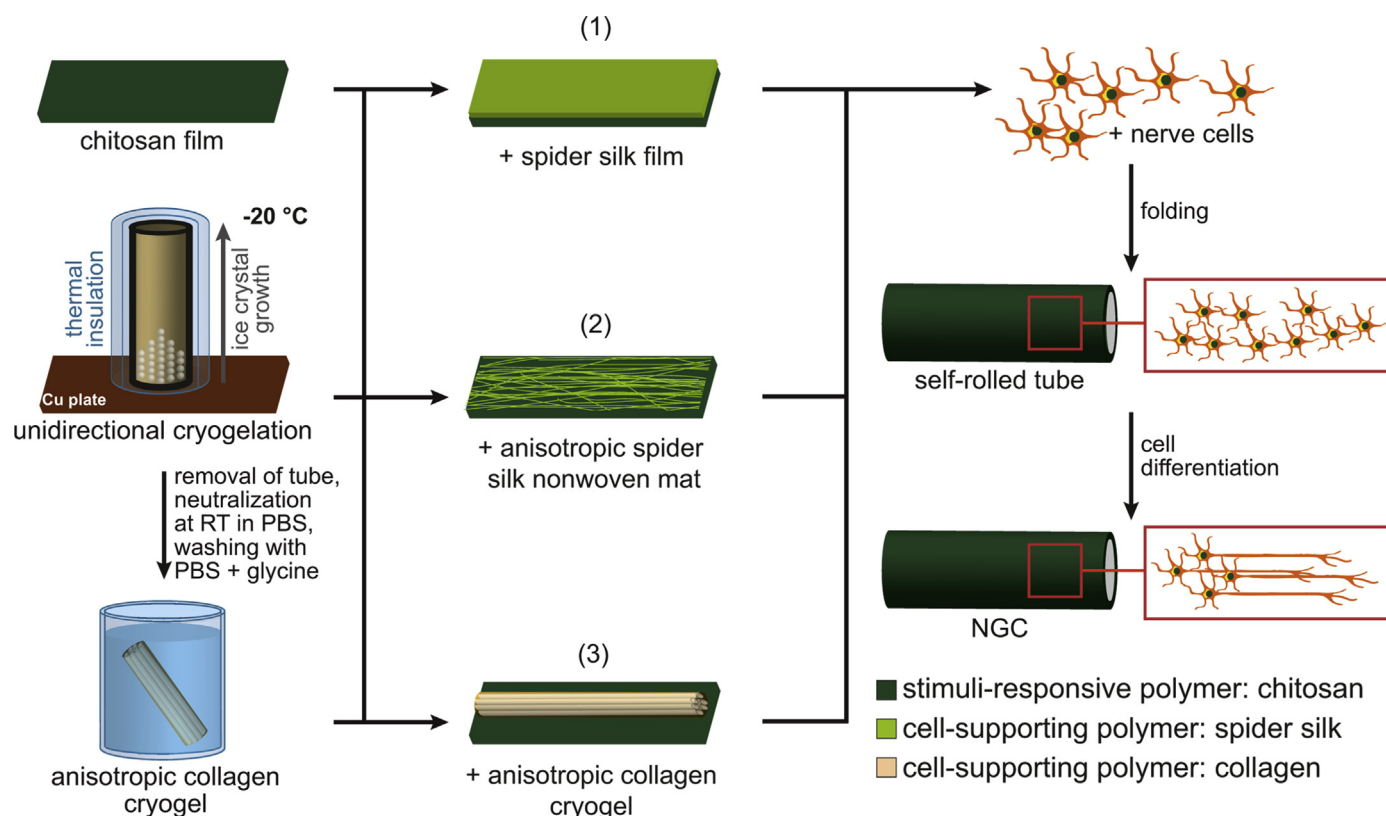
Fig. 1. Nerve guidance conduit (NGC) fabrication. Chitosan sheets were modified by either (1) a film on top of the inner wall made of the recombinant spider silk protein eADF4(C16)-RGD, (2) a layer of an anisotropic non-woven mat on top of the inner wall made of the recombinant spider silk protein eADF4(C16), or (3) an anisotropic collagen cryogel filling the inner volume of the tube. The collagen cryogel was produced using unidirectional cryogelation at −20 °C, followed by thawing, solvent neutralization, and several washing steps. The various NGC precursor constructs were placed in a PC-12 nerve cell suspension inducing self-rolling of the chitosan film used as the outer layer, and thereby encapsulated the cells, which had then the possibility to differentiate.
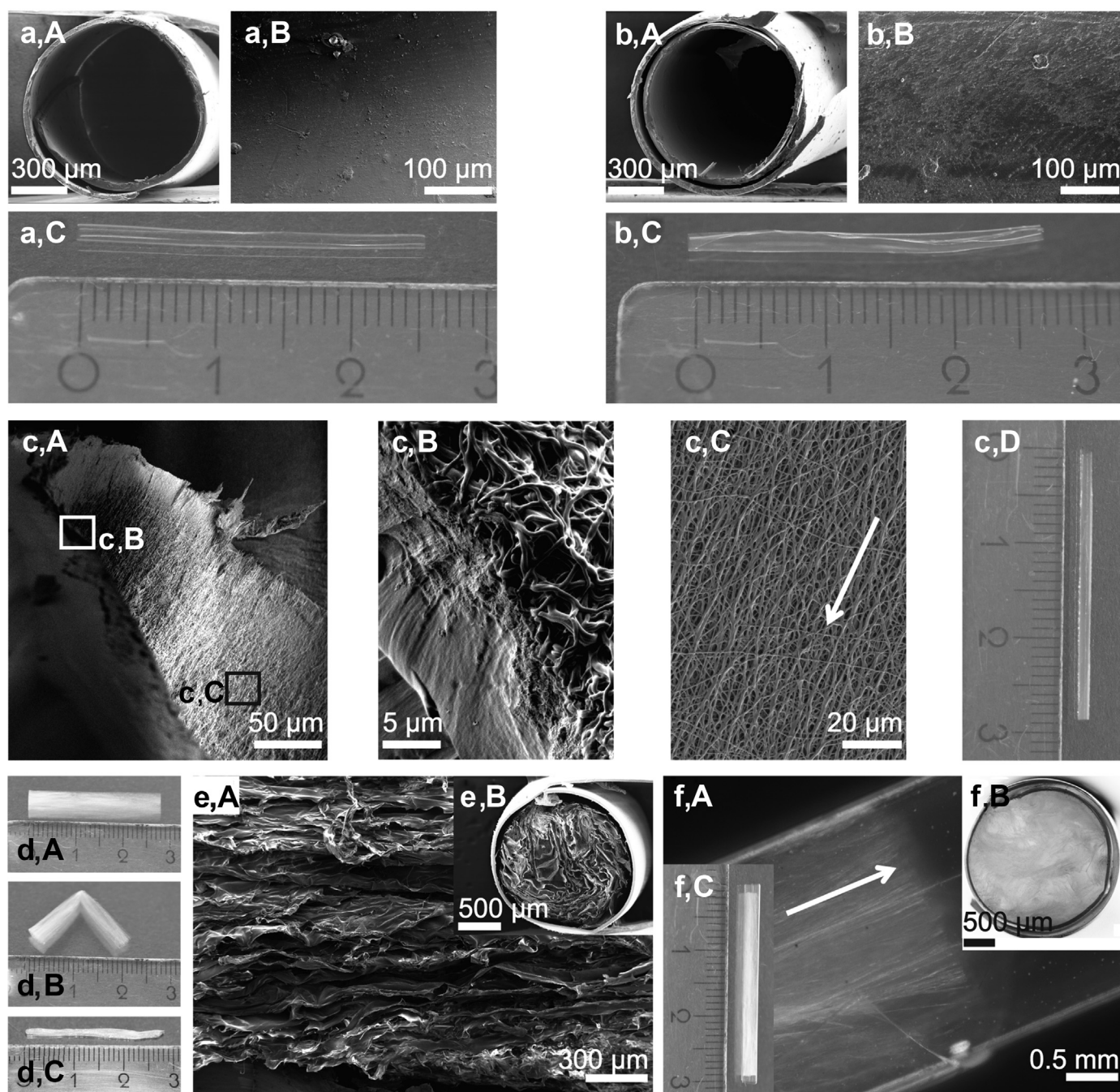
Fig. 2. Morphological characterization of NGCs. (a) (A) Scanning electron microscopy (SEM) image of the cross-section of the self-rolled chitosan tube; (B) its inner surface topography; and (C) photograph showing the whole tube after self-rolling in PBS. (b) (A) SEM image of the cross-section of the chitosan tube coated with eADF4(C16)-RGD on the inner surface (not visible here); (B) of the resulting inner surface topography; and (C) photograph showing the whole tube after self-rolling in PBS. (c) (A) SEM image of a chitosan tube comprising an inner lining with an anisotropic non-woven mat made of eADF4(C16); (B) magnified image of (c) (A) (white box): The chitosan tube and the non-woven mat are physically connected because of the processing conditions. (c) (C) Magnified image of (c) (A) (black box): The eADF4(C16) non-woven nanofibers were deposited on the chitosan inner surface in an anisotropic manner (the white arrow indicates the direction of nanofiber orientation). (c) (D) Photograph showing the whole tube after self-rolling in PBS. (d) (A) Photograph of a collagen cryogel stored in PBS; (B) Bending of the collagen cryogel in PBS resulted in a sharp bending edge indicating its anisotropic character; and (C) PBS removal from a collagen cryogel yielded a significant volume reduction. (e) (A) SEM image of a freeze-dried collagen cryogel and (B) its cross-section in the chitosan tube. (f) (A) Stereo microscopy image of the anisotropic collagen cryogel within a chitosan tube and (B) of its cross-section; (C) photograph of the chitosan tube filled with the anisotropic collagen cryogel. NGCs, nerve guidance conduits; PBS, phosphate buffered saline.

post-treated eADF4(C16)-RGD film at low pH values, compared with other biopolymers such as collagen, prevented its resolubilization when the acidic chitosan solution was cast thereon during fabrication. The eADF4(C16)-RGD layer exhibited a smooth surface topography (Fig. 2b,B). Owing to the preparation procedure of the bilayer, the eADF4(C16)-RGD layer was physically cross-linked with the chitosan layer [49]. This bilayer tube was slightly turbid (Fig. 2b,C) compared with the plain chitosan tube.

The second NGC variant had an anisotropic non-woven mat as a cell guiding element on the inner tube wall (Fig. 2c,A). Owing to the post-

treatment during tube fabrication, the chitosan surface was molten with the non-woven mat preventing delamination (Fig. 2c,B). The silk fibers with diameters ranging from 0.5 to 1.0 μm were longitudinally oriented (Fig. 2c,C) because of the processing condition (Section 2.3) and led to slight turbidity of the tube (Fig. 2c,D). Importantly, the low thickness of both, the spider silk film and the non-woven mat, was negligible in comparison with that of the chitosan layer. Therefore, no differences in the rolling behavior and only minuscule differences in bilayer thickness were observed (data not shown).

The third NGC was fabricated slightly differently: the tubular collagen cryogels were stored in PBS buffer, transferred to the PC-12 cell suspension, and enclosed with the self-rolling chitosan film. Upon bending the tubular cryogels, sharp edges appeared indicative of having anisotropic features within this material (Fig. 2d,A and B). The bending was observed to be fully reversible. Furthermore, removing all unbound water showed the high water absorption capacity of the collagen cryogels (Fig. 2d,C). The water content of the collagen cryogels, when fully soaked in PBS, was determined to be $90.7 \pm 1.4\%$ (w/w). Accordingly, the collagen cryogels showed an 11-fold volume increase during swelling. A closer look onto the surface of freeze-dried collagen cryogels using SEM revealed longitudinally oriented structures (Fig. 2e,A), and a lamellar structure could be observed in the cross-section (Fig. 2e,B). The anisotropic structure was well maintained after rolling (Fig. 2f,A), and the cryogel completely filled the chitosan tube lumen (Fig. 2f,B). Fig. 2f,C shows a photograph of the cryogel within the chitosan tube.

The chitosan films and the collagen cryogels were analyzed in wet/moist state using tensile testing. Because fully PBS-soaked collagen cryogels were observed to lose their unbound water during fixation, we removed the water in advance using a paper tissue, thereby ensuring a defined cross-sectional area for tensile property calculation. The tensile strength, maximum strain, and Young's modulus were determined to be 47 ± 17 MPa, $101 \pm 24\%$, and 30 ± 13 MPa for wet chitosan films, and 0.15 ± 0.04 MPa, $70 \pm 7\%$, and 0.22 ± 0.04 MPa for moist collagen cryogels, respectively, (values for rabbit tibial nerves are: 11.7 ± 0.7 MPa tensile strength and $38.5 \pm 2\%$ maximum strain [54]). Both the films and the cryogels showed large ramps of linear elastic deformation. In contrast to films, cryogels did not show a sharp material rupture but showed a gradual deformation after reaching the yield point (Supplementary Fig. S1). The deformation process of the cryogels continued up to 300% strain until no more force was detected. Importantly, the Young's modulus of the moist cryogels was in the range of that of peripheral nerve tissue (0.15–0.3 MPa) [55], presumably yielding a suitable environment for
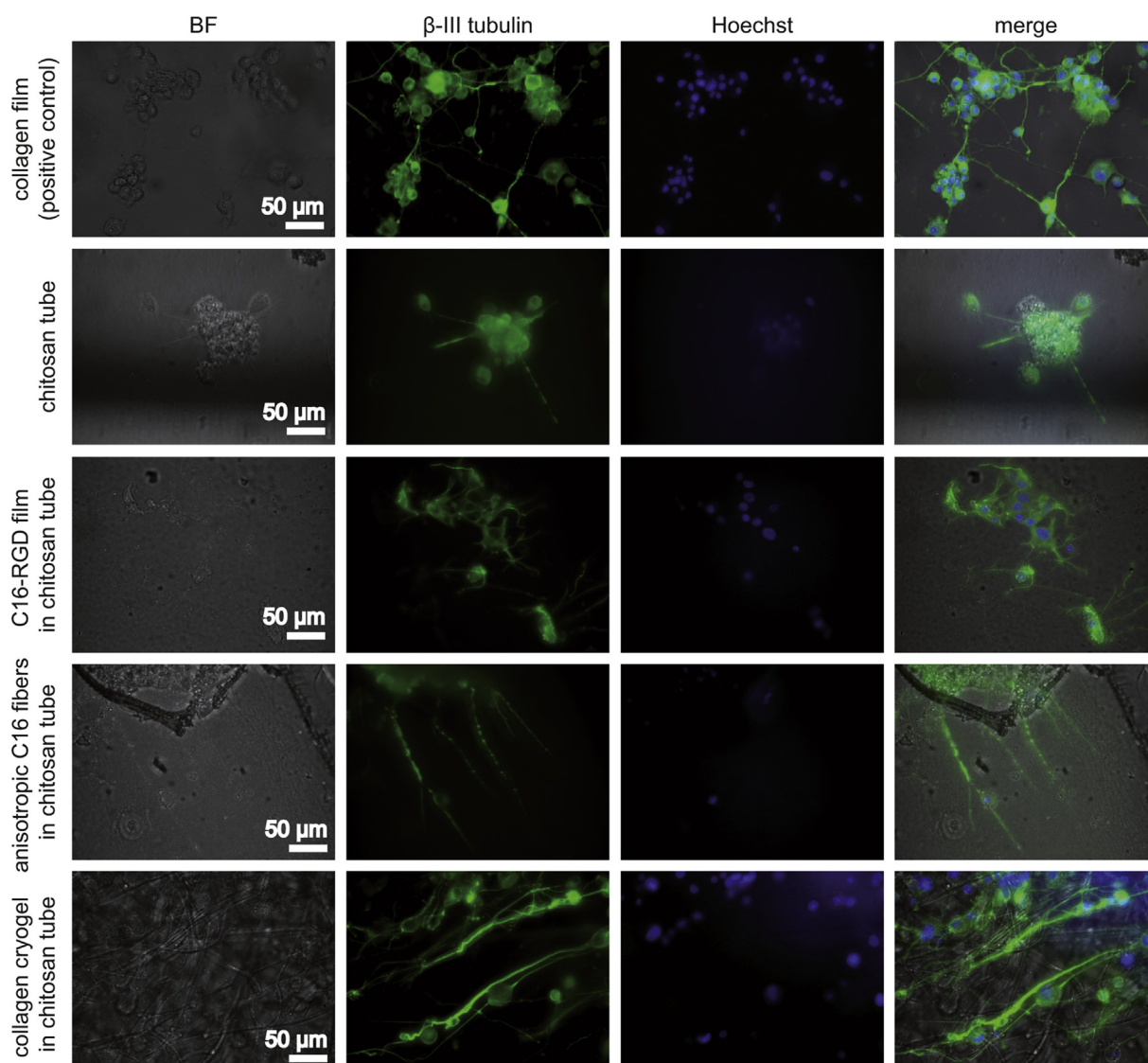
Fig. 3. Investigation of PC-12 nerve cell differentiation on all materials in tubes used in this study at day 7. A collagen film was used as a positive control for differentiation. Brightfield (BF) imaging showed the general material appearance; immunostaining against β-III tubulin (green) visualized the microtubule-forming protein present in differentiated neurons; Hoechst (blue) staining visualized cell nuclei. All images are at the same scale. C16, eADF4(C16)

nerve cells, while the chitosan film could provide stability during and after implantation, as well as structural integrity of the filler material and cells.

### 3.2. Differentiation of neuronal cells on individual materials

According to Orlowska et al. [56], attachment of PC-12 cells to polystyrene tissue culture flasks/plates is poor at laboratory conditions, and the cells form floating aggregates and grow in clusters [57]. Furthermore, this weak cell adhesion results in poor differentiation and insufficient levels of neurite outgrowth [57]. In agreement with Kleinman et al. [58], we therefore used collagen type I to coat the surface of our plates, yielding improved PC-12 cell attachment. Consequently, this coating was used as a positive control in our experiments. The suitability of the three different tube modifications in terms of PC-12 nerve cell adhesion was first investigated on plain materials individually. As it is shown in Supplementary Fig. S2, PC-12 cells equivalently adhered on a collagen film (positive control), an eADF4(C16)-RGD film, an eADF4(C16) spider silk non-woven mat, and on an anisotropic collagen cryogel. We did not observe any differences in terms of cell attachment or floating aggregates between these samples in comparison with the positive control within 7 days of culture.

PC-12 cells further possess the ability to differentiate upon lowering the serum content and adding NGFs [59]. This factor helps to protect neurons against camptothecin, serum deprivation, and etoposide-induced cell death. PC-12 cells offer advantages in comparison with cultured primary cortical neurons, including the ability to differentiate and show neurite formation. Studies have shown that a specific signaling pathway including the mitogen-activated protein kinase is the major mediator of PC-12 differentiation in response to NGFs. However, more signaling pathways are activated by the NGF, which is reviewed in

detail [60]. Therefore, in a second experiment, the growth medium was exchanged with differentiation medium on day 2, and cells were then monitored for seven days. Since the specific doubling time of these nerve cells is 48 h [52], they were first given time to adhere to the surface without proliferation before initiating differentiation. Cells were immunostained for β-III tubulin expression, which is a microtubule-forming protein produced in the early differentiation phase of neuronal cells [61]. On all substrates, the majority of the cells differentiated as indicated by the formation of neurites (Supplementary Fig. S3). Although cells on eADF4(C16)-RGD films showed only few and short neurites, the positive β-III tubulin staining confirmed that the cells started to differentiate. Both, the collagen film and the eADF4(C16) non-woven mat showed clear neurite outgrowth. Remarkably, nerve cells cultured and differentiated on collagen cryogels showed a high number of neurites, which were aligned with the underlying structures and they were interacting with other neurites forming bundles (Supplementary Fig. S4).

3.3. Entrapment of neuronal cells in NGCs

PC-12 cells were entrapped in the self-rolling NGCs by allowing the rolling process to occur directly in cell suspension. Thereby, the cells were distributed homogeneously throughout the tube and they were subsequently induced to differentiate for seven days (Fig. 3). Pure chitosan tubes showed poor cell adhesion, and aggregated cell clusters indicated that chitosan tubes did not promote effective cell adhesion. In contrast, chitosan tubes modified with an eADF4(C16)-RGD film coating showed good cell adhesion and isotropic neurite outgrowth similar to that on collagen films (Figs. 3 and 4A, B) because no guidance cue was provided in both cases. Chitosan tubes lined with anisotropic eADF4(C16) non-woven mats yielded adhered and differentiated PC-
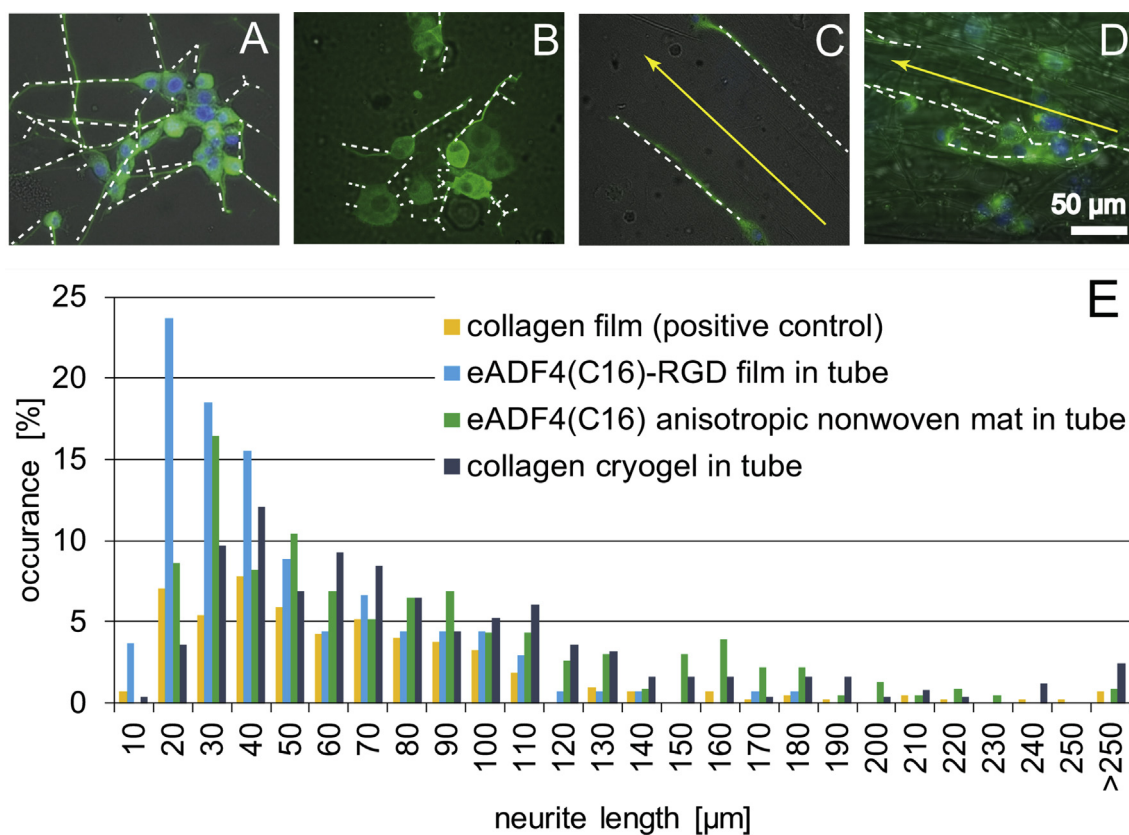
Fig. 4. Analysis of neurite lengths grown on the materials used in this study. Neurites are marked with white lines to highlight their direction of outgrowth. (A) On a collagen film (positive control) and (B) on an eADF4(C16)-RGD film, neurites grew isotropically, whereas (C) an anisotropic eADF4(C16) non-woven mat and (D) an anisotropic collagen cryogel allowed guidance of neurites into longitudinal direction. Yellow arrows indicate the orientation of anisotropic structures observed in the eADF4(C16) non-woven mat and in the collagen cryogel. (E) Neurite length distribution as detected on the materials used.

12 cells, which aligned with the nanofibers (Figs. 3 and 4C). The anisotropic collagen cryogels also allowed PC-12 cell adhesion and differentiation, and neurites followed their longitudinally oriented structure (Figs. 3 and 4D). To image the cells within the cryogels, they were cut into slices. The presence of cells within the interior of the cryogel confirmed that cells were able to migrate into the lamellar structures and that they spread their neurites longitudinally within the cryogels. Moreover, it can be assumed that sufficient perfusion of nutrients, oxygen, and waste metabolites throughout the cryogel supported the viability and differentiation of the cells. The spreading of long and parallel neurites within the lamellar structures of the cryogels is depicted in Fig. 3 and Fig. S4.

Next, neurite lengths were measured and the quantitative distribution of their lengths was determined. Therein, '10 μm' includes all neurites with a length ranging from 0 to 10 μm, '20 μm' includes all neurites with a length between 10 and 20 μm, and so on (Fig. 4E). NGCs comprising either an anisotropic eADF4(C16) non-woven mat or a collagen cryogel, as well as the collagen film (positive control) promoted outgrowth of neurites with lengths exceeding 250 μm. However, the longest neurites in the NGCs with an eADF4(C16)-RGD film were shown to have a length of 180 μm. Further, it could be observed that NGCs modified with an eADF4(C16)-RGD film showed the highest occurrence of neurite length in the range of 10–20 μm and, therefore, seemed to lead to the shortest neurites in this test. The chitosan tube with aligned eADF4(C16) non-woven mats peaked at 20–30 μm neurite length. The collagen film and constructs comprising the collagen cryogel exhibited most neurites at a length of 30–40 μm, hence, double the length as observed in eADF4(C16)-RGD–modified constructs. Most of the neurites longer than 250 μm were found in the collagen cryogel, which is remarkable, because the neurites in these samples could only be determined in a thin z-layer. Therefore, it can be assumed that the actual neurite length could be even longer.

To determine neurite length per cell, the number of cells in each image was counted. Cells on collagen films showed an average neurite length of 16 μm, 19 μm on eADF4(C16)-RGD films within a tube, 34 μm on eADF4(C16) anisotropic non-woven mats within a tube, and 47 μm on collagen cryogels within tube. This result further indicates the suitability of collagen cryogels encapsulated in self-rolled tubes as a promising candidate serving as an NGC.

4. Conclusions

Self-rolling tubes made of chitosan are beneficial for designing NGCs, because they enable gentle encapsulation of neuronal cells and the dedicated modification of the inner tube wall or its lumen with supporting materials, such as a bioactive recombinant spider silk film, an anisotropic recombinant spider silk non-woven mat, or an anisotropic collagen cryogel. All tube modifications were shown to be functional concerning enhancement of nerve cell attachment and differentiation. Anisotropic non-woven mats and collagen cryogels even supported guidance of neurites. This *in vitro* study opens the road toward *in vivo* studies to demonstrate the feasibility of the individual NGC or even combinations thereof and if the self-rolling properties of the NGCs will support the surgical procedure.

Author contributions

Tamara B. Aigner: Funding acquisition, Conceptualization, Methodology, Validation, Formal analysis, Investigation, Data curation, Writing - Original draft, Writing - Review and Editing, Visualization. Christian Haynl: Conceptualization, Methodology, Validation, Formal analysis, Investigation, Data curation, Writing - Original draft, Writing - Review and Editing, Visualization. Sahar Salehi: Funding acquisition, Conceptualization, Methodology, Validation, Writing - Review and Editing, Visualization. Andrea O'Connor: Funding acquisition, Writing – Review & Editing. Thomas Scheibel: Supervision, Funding acquisition, Writing – Review & Editing.

Declaration of competing interest

The authors declare that they have no known competing financial interests or personal relationships that could have appeared to influence the work reported in this paper.

Appendix A. Supplementary data

Supplementary data to this article can be found online at https://doi.org/10.1016/j.mtbio.2020.100042.

References

[1] L.R. Robinson, Traumatic injury to peripheral nerves, Muscle Nerve 23 (6) (2000) 863–873.
[2] W. Daly, L. Yao, D. Zeugolis, A. Windebank, A. Pandit, A biomaterials approach to peripheral nerve regeneration: bridging the peripheral nerve gap and enhancing functional recovery, J. R. Soc. Interface 9 (67) (2012) 202–221.
[3] A. Magaz, A. Faroni, J.E. Gough, A.J. Reid, X. Li, J.J. Blaker, Bioactive silk-based nerve guidance conduits for augmenting peripheral nerve repair, Adv. Healthc. Mater. 7 (23) (2018) 1800308.
[4] E.G. Fine, I. Decosterd, M. Papaloïzos, A.D. Zurn, P. Aebischer, GDNF and NGF released by synthetic guidance channels support sciatic nerve regeneration across a long gap, Eur. J. Neurosci. 15 (4) (2002) 589–601.
[5] G. Lundborg, L.B. Dahlin, N. Danielsen, R.H. Gelberman, F.M. Longo, H.C. Powell, et al., Nerve regeneration in silicone chambers: influence of gap length and of distal stump components, Exp. Neurol. 76 (2) (1982) 361–375.
[6] N.P. Patel, K.A. Lyon, J.H. Huang, An update-tissue engineered nerve grafts for the repair of peripheral nerve injuries, Neural Regen. Res. 13 (5) (2018) 764–774.
[7] W.Z. Ray, S.E. Mackinnon, Management of nerve gaps: autografts, allografts, nerve transfers, and end-to-side neurorrhaphy, Exp. Neurol. 223 (1) (2010) 77–85.
[8] A. Berger, H. Millesi, Nerve grafting, Clin. Orthop. Relat. Res. 133 (1978) 49–55.
[9] A.M. Ghaznavi, L.E. Kokai, M.L. Lovett, D.L. Kaplan, K.G. Marra, Silk fibroin conduits: a cellular and functional assessment of peripheral nerve repair, Ann. Plast. Surg. 66 (3) (2011) 273–279.
[10] S.K. Lee, S.W. Wolfe, Peripheral nerve injury and repair, JAAOS - J. Am. Acad. Orthop.Surg. 8 (4) (2000) 243–252.
[11] P.A. Wieringa, A.R. Goncalves De Pinho, S. Micera, R.J.A. Van Wezel, L. Moroni, Biomimetic architectures for peripheral nerve repair: a review of biofabrication strategies, Adv. Healthc. Mater. 7 (8) (2018), e1701164.
[12] W.A. Lackington, A.J. Ryan, F.J. O'brien, Advances in nerve guidance conduit-based therapeutics for peripheral nerve repair, ACS Biomater. Sci. Eng. 3 (7) (2017) 1221–1235.
[13] G.C.W. De Ruiter, M.J.A. Malessy, M.J. Yaszemski, A.J. Windebank, R.J. Spinner, Designing ideal conduits for peripheral nerve repair, Neurosurg, Focus 26 (2) (2009). E5-E5.
[14] S. Kehoe, X.F. Zhang, D. Boyd, FDA approved guidance conduits and wraps for peripheral nerve injury: a review of materials and efficacy, Injury 43 (5) (2012) 553–572.
[15] T.M.A. Henderson, K. Ladewig, D.N. Haylock, K.M. Mclean, A.J. O'connor, Cryogels for biomedical applications, J. Mater. Chem. B 1 (21) (2013) 2682–2695.
[16] T.M. Henderson, K. Ladewig, D.N. Haylock, K.M. Mclean, A.J. O'connor, Formation and characterisation of a modifiable soft macro-porous hyaluronic acid cryogel platform, J. Biomater. Sci. Polym. Ed. 26 (13) (2015) 881–897.
[17] D. Arslantunali, T. Dursun, D. Yucel, N. Hasirci, V. Hasirci, Peripheral nerve conduits: technology update, Med. Devices (Auckl) 7 (2014) 405–424.
[18] G. Koopmans, B. Hasse, N. Sinis, The role of collagen in peripheral nerve repair, Int. Rev. Neurobiol. 87 (2009) 363–379.

[19] T. Ushiki, C. Ide, Three-dimensional organization of the collagen fibrils in the rat sciatic nerve as revealed by transmission- and scanning electron microscopy, Cell Tissue Res. 260 (1) (1990) 175–184.

[20] A. Sorushanova, L.M. Delgado, Z.N. Wu, N. Shologu, A. Kshirsagar, R. Raghunath, et al., The collagen suprafamily: from biosynthesis to advanced biomaterial development, Adv. Mater. 31 (1) (2019), 1801651.

[21] K.L. Lin, D.W. Zhang, M.H. Macedo, W.G. Cui, B. Sarmento, G.F. Shen, Advanced collagen-based biomaterials for regenerative biomedicine, Adv. Funct. Mater. 29 (3) (2019) 1804943.

[22] R.C. Goy, S.T.B. Morais, O.B.G. Assis, Evaluation of the antimicrobial activity of chitosan and its quaternized derivative on E. coli and S. aureus growth, Rev. Bras. de Farmacogn. 26 (1) (2016) 122–127.

[23] M. Rinaudo, Chitin and chitosan: properties and applications, Prog. Polym. Sci. 31 (7) (2006) 603–632.

[24] D.P. Biswas, P.A. Tran, C. Tallon, A.J. O'connor, Combining mechanical foaming and thermally induced phase separation to generate chitosan scaffolds for soft tissue engineering, J. Biomater. Sci. Polym. Ed. 28 (2) (2017) 207–226.

[25] M.J. Simoes, A. Gartner, Y. Shirosaki, R.M. Gil Da Costa, P.P. Cortez, F. Gartner, et al., In vitro and in vivo chitosan membranes testing for peripheral nerve reconstruction, Acta Med. Port. 24 (1) (2011) 43–52.

[26] Q. Guo, C. Liu, B. Hai, T. Ma, W. Zhang, J. Tan, et al., Chitosan conduits filled with simvastatin/Pluronic F-127 hydrogel promote peripheral nerve regeneration in rats, J. Biomed. Mater. Res. B Appl. Biomater. 106 (2) (2018) 787–799.

[27] T.A. Blackledge, C.Y. Hayashi, Silken toolkits: biomechanics of silk fibers spun by the orb web spider Argiope argentata (Fabricius 1775), J. Exp. Biol. 209 (13) (2006) 2452–2461.

[28] F. Vollrath, D. Porter, Spider silk as archetypal protein elastomer, Soft Matter 2 (5) (2006) 377–385.

[29] C. Radtke, C. Allmeling, K.H. Waldmann, K. Reimers, K. Thies, H.C. Schenk, et al., Spider silk constructs enhance axonal regeneration and remyelination in long nerve defects in sheep, PloS One 6 (2) (2011), e16990.

[30] C. Allmeling, A. Jokuszies, K. Reimers, S. Kall, C.Y. Choi, G. Brandes, et al., Spider silk fibres in artificial nerve constructs promote peripheral nerve regeneration, Cell Prolif 41 (3) (2008) 408–420.

[31] K. Schacht, T. Scheibel, Processing of recombinant spider silk proteins into tailor-made materials for biomaterials applications, Curr. Opin. Biotechnol. 29 (2014) 62–69.

[32] M. Lewicka, O. Hermanson, A.U. Rising, Recombinant spider silk matrices for neural stem cell cultures, Biomaterials 33 (31) (2012) 7712–7717.

[33] B. An, M.D. Tang-Schomer, W.W. Huang, J.Y. He, J.A. Jones, R.V. Lewis, et al., Physical and biological regulation of neuron regenerative growth and network formation on recombinant dragline silks, Biomaterials 48 (2015) 137–146.

[34] K. Pawar, G. Welzel, C. Haynl, S. Schuster, T. Scheibel, Recombinant spider silk and collagen-based nerve guidance conduits support neuronal cell differentiation and functionality in vitro, ACS Appl. Bio Mater. 2 (11) (2019) 4872–4880.

[35] T.B. Aigner, E. Desimone, T. Scheibel, Biomedical applications of recombinant silk-based materials, Adv. Mater. 30 (19) (2018), e1704636.

[36] K. Schacht, T. Jüngst, M. Schweinlin, A. Ewald, J. Groll, T. Scheibel, Biofabrication of cell-loaded 3D spider silk constructs, Angew. Chem. Int. Ed. 54 (9) (2015) 2816–2820.

[37] K. Schacht, J. Vogt, T. Scheibel, Foams made of engineered recombinant spider silk proteins as 3D scaffolds for cell growth, ACS Biomater. Sci. Eng. 2 (4) (2016) 517–525.

[38] A. Leal-Egana, G. Lang, C. Mauerer, J. Wickinghoff, M. Weber, S. Geimer, et al., Interactions of fibroblasts with different morphologies made of an engineered spider silk protein, Adv. Eng. Mater. 14 (3) (2012) B67–B75.

[39] C.B. Borkner, S. Wohlrab, E. Moller, G. Lang, T. Scheibel, Surface modification of polymeric biomaterials using recombinant spider silk proteins, ACS Biomater. Sci. Eng. 3 (5) (2017) 767–775.

[40] C.B. Borkner, M.B. Elsner, T. Scheibel, Coatings and films made of silk proteins, ACS Appl. Mater. Interfaces 6 (18) (2014) 15611–15625.

[41] E. Desimone, K. Schacht, A. Pellert, T. Scheibel, Recombinant spider silk-based bioinks, Biofabrication 9 (4) (2017), 044104.

[42] D. Steiner, G. Lang, L. Fischer, S. Winkler, T. Fey, P. Greil, et al., Intrinsic vascularization of recombinant eADF4(C16) spider silk matrices in the arteriovenous loop model, Tissue Eng. Part A (2019) 1504–1513.

[43] P.H. Zeplin, N.C. Maksimovikj, M.C. Jordan, J. Nickel, G. Lang, A.H. Leimer, et al., Spider silk coatings as a bioshield to reduce periprosthetic fibrous capsule formation, Adv. Funct. Mater. 24 (18) (2014) 2658–2666.

[44] P.H. Zeplin, A.K. Berninger, N.C. Maksimovikj, P. Van Gelder, T. Scheibel, H. Walles, Improving the biocompatibility of silicone implants using spider silk coatings: immunohistochemical analysis of capsule formation, Handchir. Mikrochir. Plast. Chir. 46 (6) (2014) 336–341.

[45] T.I. Harris, D.A. Gaztambide, B.A. Day, C.L. Brock, A.L. Ruben, J.A. Jones, et al., Sticky situation: an investigation of robust aqueous-based recombinant spider silk protein coatings and adhesives, Biomacromolecules 17 (11) (2016) 3761–3772.

[46] S. Müller-Herrmann, T. Scheibel, Enzymatic degradation of films, particles, and nonwoven meshes made of a recombinant spider silk protein, ACS Biomater. Sci. Eng. 1 (4) (2015) 247–259.

[47] B. Zhu, W. Li, R.V. Lewis, C.U. Segre, R. Wang, E-spun composite fibers of collagen and dragline silk protein: fiber mechanics, biocompatibility, and application in stem cell differentiation, Biomacromolecules (2014) 202–213.

[48] S. Wohlrab, S. Müller, A. Schmidt, S. Neubauer, H. Kessler, A. Leal-Egana, et al., Cell adhesion and proliferation on RGD-modified recombinant spider silk proteins, Biomaterials 33 (28) (2012) 6650–6659.

[49] T. Aigner, T. Scheibel, Self-rolling refillable tubular enzyme containers made of recombinant spider silk and chitosan, ACS Appl. Mater. Interfaces 11 (17) (2019) 15290–15297.

[50] G. Lang, Herstellung und Charakterisierung von Fasern aus rekombinanten Spinnenseidenproteinen und deren potentielle Applikationen, 2015. Dissertation, urn:nbn:de:bvb:703-epub-2038-3. (Accessed 15 July 2019).

[51] L. Ionov, Soft microorigami: self-folding polymer films, Soft Matter 7 (15) (2011) 6786–6791.

[52] ATCC, PC-12 (ATCC® CRL-1721™), 2016. https://www.lgcstandards-atcc.org/products/all/CRL-1721.aspx?geo_country=de#specifications. (Accessed 6 August 2019).

[53] M. Sarker, S. Naghieh, A.D. Mcinnes, D.J. Schreyer, X. Chen, Strategic design and fabrication of nerve guidance conduits for peripheral nerve regeneration, Biotechnol. J. 13 (7) (2018), 1700635.

[54] M.K. Kwan, E.J. Wall, J. Massie, S.R. Garfin, Strain, stress and stretch of peripheral nerve Rabbit experiments in vitro and in vivo, Acta Orthop. Scand. 63 (3) (1992) 267–272.

[55] J.B. Scott, M. Afshari, R. Kotek, J.M. Saul, The promotion of axon extension in vitro using polymer-templated fibrin scaffolds, Biomaterials 32 (21) (2011) 4830–4839.

[56] A. Orlowska, P.T. Perera, M. Al Kobaisi, A. Dias, H.K.D. Nguyen, S. Ghanaati, et al., The effect of coatings and nerve growth factor on attachment and differentiation of pheochromocytoma cells, Materials (Basel) 11 (1) (2017) 60.

[57] D.G. Attiah, R.A. Kopher, T.A. Desai, Characterization of PC12 cell proliferation and differentiation-stimulated by ECM adhesion proteins and neurotrophic factors, J. Mater. Sci. Mater. Med. 14 (11) (2003) 1005–1009.

[58] H.K. Kleinman, L. Luckenbill-Edds, F.W. Cannon, G.C. Sephel, Use of extracellular matrix components for cell culture, Anal. Biochem. 166 (1) (1987) 1–13.

[59] N. Kinarivala, K. Shah, T.J. Abbruscato, P.C. Trippier, Passage variation of PC12 cells results in inconsistent susceptibility to externally induced apoptosis, ACS Chem. Neurosci. 8 (1) (2017) 82–88.

[60] E.J. Huang, L.F. Reichardt, Trk receptors: roles in neuronal signal transduction, Annu. Rev. Biochem. 72 (1) (2003) 609–642.

[61] M.A. Tischfield, H.N. Baris, C. Wu, G. Rudolph, L. Van Maldergem, W. He, et al., Human TUBB3 mutations perturb microtubule dynamics, kinesin interactions, and axon guidance, Cell 140 (1) (2010) 74–87.